

A SEMIGROUP METHOD FOR HIGH DIMENSIONAL ELLIPTIC PDES AND EIGENVALUE PROBLEMS BASED ON NEURAL NETWORKS

HAOYA LI AND LEXING YING

ABSTRACT. In this paper, we propose a semigroup method for solving high-dimensional elliptic partial differential equations (PDEs) and the associated eigenvalue problems based on neural networks. For the PDE problems, we reformulate the original equations as variational problems with the help of semigroup operators and then solve the variational problems with neural network (NN) parameterization. The main advantages are that no mixed second-order derivative computation is needed during the stochastic gradient descent training and that the boundary conditions are taken into account automatically by the semigroup operator. For eigenvalue problems, a primal-dual method is proposed, resolving the constraint with a scalar dual variable. Numerical results are provided to demonstrate the performance of the proposed methods.

1. INTRODUCTION

Central to the discipline of applied mathematics is the problem of numerically solving partial differential equations (PDEs), among which the high dimensional problems are particularly challenging due to the “curse of dimensionality”, a phenomenon that the computational complexity of certain algorithms increases exponentially with the dimension. A more challenging problem is the eigenvalue problem, which is closely related with the PDE problem and suffers from the curse of dimensionality as well. In this paper we limit the discussion to second-order linear PDEs and related eigenvalue problems.

In recent years, deep learning methods have experienced great success across a wide range of domains such as image recognition [9, 14], natural language processing [3, 7], molecular dynamics simulation [10, 17], and protein structure prediction [1]. One reason behind this success is that neural network models are good approximators for high-dimensional functions that can be trained efficiently in most cases. Leveraging on this property of the neural network, a myriad of data-driven methods have been proposed for solving high-dimensional PDEs and eigenvalue problems, for example, see [4, 5, 15, 16].

In a recent paper [15], the semigroup operator of the differential operator is used to rewrite the variational form, which frees the algorithm from calculations of any mixed second-order derivative and automatically handles the boundary conditions. In this paper, we extend this method to more general elliptic PDEs and also derive a primal-dual method for solving the corresponding eigenvalue problems.

1.1. Background and related work. For high-dimensional PDEs, Monte-Carlo methods using Feynman-Kac formulas can be applied to obtain the value of the approximate solution at a given location. However, satisfactory solutions should provide information of not only the values on a finite number of points, but also of the entire landscape.

Monte Carlo methods have also been widely applied to the eigenvalue problems. Among various approaches, the variational Monte Carlo method (VMC) and the diffusion Monte Carlo method (DMC) are two most well-known examples that have been thoroughly investigated in the context of quantum mechanics, see for example [6]. The idea of VMC is to parameterize the wave function and

Key words and phrases. Partial differential equation, eigenvalue problem, neural network, semigroup method. Department of Mathematics, Stanford University, Stanford, CA 94305, USA (lihaoya@stanford.edu).

Department of Mathematics and ICME, Stanford University, Stanford, CA 94305, USA (lexing@stanford.edu).

The work of L.Y. is partially supported by the U.S. Department of Energy, Office of Science, Office of Advanced Scientific Computing Research, Scientific Discovery through Advanced Computing (SciDAC) program and also by the National Science Foundation under award DMS-1818449.

minimize the energy of the system with respect to the parameters, where the energy is expressed as an expectation with respect to the probability distribution given by the squared modulus of the wave function, and is numerically computed via the Monte Carlo method. DMC utilizes the imaginary-time Schrödinger equation, whose solution can be represented by a convolution with respect to the Green's function and can thus be evaluated by Monte Carlo simulations. Since the imaginary-time Schrödinger equation is a linear differential equation, the component of the lowest energy eigenfunction remains and other components vanish as the time goes to infinity, and the wave function of the ground state can be obtained.

For neural network based approaches, the general idea is to approximate the solution with a neural network, and then train the neural network to minimize a loss built either from a variational form of the PDE or from a norm of the residue of an equivalent equation of the original PDE. Mostly related to the current work, [11, 15] are concerned with the high dimensional PDEs describing the committor function in the transition path theory, which is a second-order elliptic equation with a specific kind of Dirichlet boundary conditions.

In [4], the backward stochastic differential equation (BSDE) method forms the equivalent equation using a BSDE, and the residue norm of the equivalent fixed-point equation is minimized. In some cases the equivalent variational problem has been established, and we only need to directly apply the neural network parameterization. For example, in [2], a neural network with one hidden layer is used to give the trial functions for the VMC method, and the gradient function needed in the optimization is also evaluated by Monte Carlo method. In [5], a ResNet structure is used to parameterize the approximate solution, and the optimization problem is obtained from the variational formulation of elliptic PDEs, which is then solved by stochastic gradient descent (SGD) methods.

In [8], the authors extend the BSDE approach to solve the eigenvalue problem with a second-order elliptic operator. The differential equation is rewritten as a fixed-point equation with the help of the corresponding semi-group operator as in the BSDE method. By Itô's formula, the semi-group operator is represented by a stochastic integral. After that, the numerical solution is obtained by minimizing the loss defining as the L^2 norm of the fixed-point equation residue. The L^2 constraint on the eigenfunction is implemented by dividing the L^2 norm in each batch during training.

Since both the proposed method and the BSDE method involves semigroups of diffusion processes, we remark that there are several major difference between the proposed method and the BSDE method. Since the BSDE method has many variants, here we take the version in [8] to avoid ambiguity. Firstly, the BSDE method usually requires two neural networks, one for the approximate solution and another for its gradient, while our method only needs a single neural network for the approximate solution. Secondly, the semigroup used in [8] is not the one that corresponds to the second-order differential parameter. In particular, it depends on λ , while in our method the semigroup does not depend on λ . Finally, in the method of [8], the eigenvalue is also a parameter that needs to be optimized, while in our method, it does not appear as a variable of the optimization problem but can be computed easily after solving for the eigenfunction.

1.2. Contributions and contents. The two major contributions of our approach are

- The semigroup formulation removes the need of calculating any mixed second-order derivatives, and it treats the boundary conditions naturally.
- We extend the semigroup method also to the eigenvalue problem with a primal dual algorithm, which is able to efficiently enforce the constraint on the L^2 norm of the approximate solution.

The rest of the paper is organized as follows. Section 2 describes the semigroup approach for the second order elliptic PDEs. Section 3 discusses the primal-dual approach for the eigenvalue problems. Finally, numerical results are reported in Section 4.

2. ELLIPTIC PDES

Consider the following second order elliptic equation:

$$(1) \quad -\nabla \cdot (a(x)\nabla u(x)) = f(x), \quad x \in \Omega$$

where the coefficient $a(x)$ is uniformly bounded above zero. Here, we consider two types of boundary conditions: the Dirichlet boundary condition:

$$(2) \quad u(x) = r(x), \quad x \in \partial\Omega,$$

and the periodic boundary condition:

$$(3) \quad u(x) = u(x + e_i), \quad x \in \Omega = [0, 1]^d,$$

where e_i is the i -th standard basis vector in \mathbb{R}^d .

2.1. Semigroup formulation. We define $V(x) = -\log(a(x))$ and let X_t be the solution to the stochastic differential equation (SDE)

$$(4) \quad dX_t = -\nabla V(X_t)dt + \sqrt{2}dW_t, \quad X_0 = x,$$

where W_t is the standard d -dimensional Brownian motion. For a fixed small time step $\delta > 0$, we define the operator P as follows:

$$(5) \quad (Pu)(x) := \mathbb{E}^x (u(X_{\tau \wedge \delta})),$$

where \mathbb{E}^x is the expectation taken with respect to the law of the process (4), and $\tau = \infty$ if the periodic boundary condition is used, and if the Dirichlet boundary condition is used, $\tau = \tau_{\partial\Omega}$ is defined as the hitting time of $\partial\Omega$. By Dynkin's formula, for the solution u of the equation (1) we have

$$(6) \quad Pu(x) = u(x) + \mathbb{E}^x \int_0^{\tau \wedge \delta} \mathcal{A}u(X_s) ds = u(x) - \mathbb{E}^x \int_0^{\tau \wedge \delta} \frac{f}{a}(X_s) ds, \quad \forall x \in \Omega,$$

where $\mathcal{A} = \Delta - \nabla V \cdot \nabla$ is the infinitesimal generator, and thus for the solution u of the PDE (1), we have $\mathcal{A}u(x) = -f(x)/a(x)$. Following [15], Pu can be decomposed into two parts as follows:

$$(7) \quad (Pu)(x) = \mathbb{E}^x (u(X_{\tau \wedge \delta})) = \mathbb{E}^x (u(X_\delta) \mathbf{1}_{\{\delta < \tau\}}) + \mathbb{E}^x (r(X_\tau) \mathbf{1}_{\{\delta \geq \tau\}}),$$

We denote the first part of (7) as

$$(8) \quad (P^i u)(x) \equiv \mathbb{E}^x (u(X_{\tau \wedge \delta}) \mathbf{1}_{\{\delta < \tau\}}) = \mathbb{E}^x (u(X_\delta) \mathbf{1}_{\{\delta < \tau\}}),$$

where the superscript i stands for the interior contribution and the second part of (7) as

$$(9) \quad (P^b r)(x) \equiv \mathbb{E}^x (r(X_{\tau \wedge \delta}) \mathbf{1}_{\{\delta \geq \tau\}}) = \mathbb{E}^x (r(X_\tau) \mathbf{1}_{\{\delta \geq \tau\}}),$$

where the superscript b stands for the boundary contribution. With these operators, (6) can be rewritten succinctly as

$$(10) \quad (I - P^i)u(x) - (P^b r)(x) - (Tf)(x) = 0,$$

where $(Tf)(x) = \mathbb{E}^x \int_0^{\tau \wedge \delta} \frac{f}{a}(X_s) ds$. This equation can be reformulated as the following variational problem

$$(11) \quad \min_u \frac{1}{2} \int_\Omega u(x) ((I - P^i)u(x)) \rho(x) dx - \int_\Omega u(x) (P^b r(x) + Tf(x)) \rho(x) dx,$$

where $\rho(x) = a(x) / (\int_\Omega a(x) dx)$. In order to do this, we need a result from [15].

Theorem 1 [15]. P^i is a symmetric operator on $L_\rho^2(\Omega)$, in other words, $\langle u, P^i v \rangle_\rho = \langle P^i u, v \rangle_\rho$, where $\langle \cdot, \cdot \rangle_\rho$ denotes the inner product of the Hilbert space $L_\rho^2(\Omega)$.

One can show using Theorem 1 that the solution to (11) is the same as the solution to (10) in the following way. Assume that u^* is the solution to (11) and η is continuous in Ω with compact support. By plugging $u(x, \epsilon) = u^*(x) + \epsilon\eta(x)$ into (11) and taking derivative with respect to ϵ , we obtain

$$\begin{aligned}
 0 &= \frac{\partial}{\partial \epsilon} \left(\frac{1}{2} \int_{\Omega} u(x, \epsilon) ((I - P^i)u(x, \epsilon)) \rho(x) dx - \int_{\Omega} u(x, \epsilon) (P^b r(x) + T f(x)) \rho(x) dx \right) \Big|_{\epsilon=0} \\
 (12) \quad &= \int_{\Omega} \eta(x) ((I - P^i)u^*(x)) \rho(x) dx - \int_{\Omega} \eta(x) (P^b r(x) + T f(x)) \rho(x) dx \\
 &= \int_{\Omega} \eta(x) ((I - P^i)u^*(x) - P^b r(x) - T f(x)) \rho(x) dx,
 \end{aligned}$$

and thus $(I - P^i)u^*(x) - P^b r(x) - T f(x) = 0$ since this is true for any η that is continuous in Ω with compact support.

2.2. Neural network approximation. In order to address the curse of dimensionality, the function u in (11) is parameterized with a neural network u_{θ} , and the optimization problem becomes

$$(13) \quad \min_{\theta} \frac{1}{2} \int_{\Omega} u_{\theta}(x) ((I - P^i)u_{\theta}(x)) \rho(x) dx - \int_{\Omega} u_{\theta}(x) (P^b r(x) + T f(x)) \rho(x) dx.$$

When the Dirichlet boundary condition (2) is used, we solve the following penalized problem to better address the boundary condition, which is not necessary but is shown to be able to improve the performance of the algorithm.

$$(14) \quad \min_{\theta} \int_{\Omega} u_{\theta}(x) \left(\frac{1}{2} (I - P^i)u_{\theta}(x) - P^b r(x) - T f(x) \right) \rho(x) dx + c \int_{\partial\Omega} (u_{\theta}(x) - r(x))^2 d\mu(x),$$

where $\mu(x)$ is a probability measure supported on $\partial\Omega$.

The architecture of the neural network used in this situation is depicted in Figure 1. We adopt a three layer fully connected neural network with ReLU activation. Compared with [15], we do not have the singularity layer here since we do not have a temperature parameter and the singularities that appear in the situation of extremely high and extremely low temperatures no longer exist.

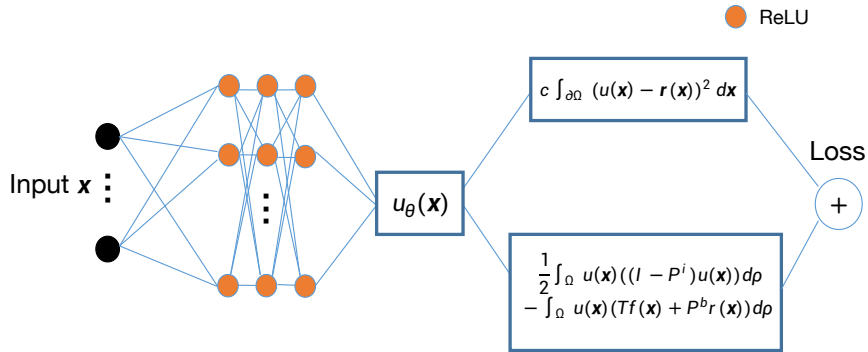


FIGURE 1. An example of the neural network architecture and the corresponding loss when using the Dirichlet boundary condition.

When the periodic boundary condition (3) is used, we adopt the following neural network architecture to address the boundary condition with the help of the trigonometric basis, where m is a hyperparameter of the neural network. Since the boundary condition is already treated by the neural network architecture, we do not need the penalty term in this situation.

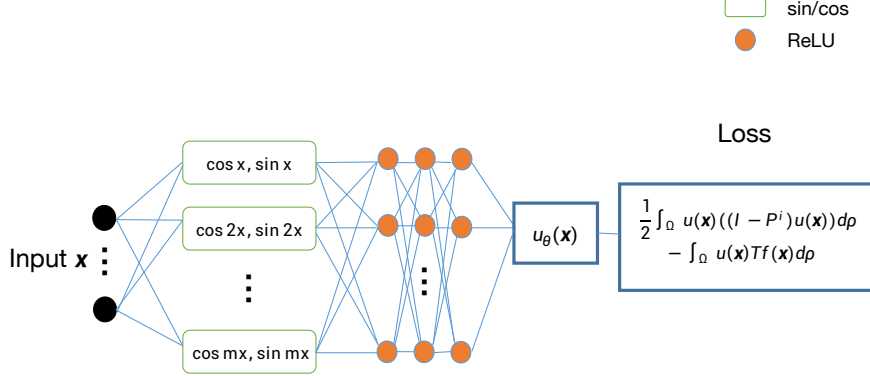


FIGURE 2. An example of the neural network architecture and the corresponding loss when using the periodic boundary condition.

In the implementation of the optimization algorithm, we also need the derivative of the integrals in (13). By the symmetry of P^i in $L^2_{\rho}(\Omega)$, the derivative is

$$(15) \quad \int_{\Omega} \nabla_{\theta} u_{\theta}(x) ((I - P^i)u_{\theta}(x)) \rho(x) dx - \int_{\Omega} \nabla_{\theta} u_{\theta}(x) (P^b r(x) + T f(x)) \rho(x) dx.$$

With the help of a random variable $X \sim \rho$, the derivative can be further transformed into:

$$(16) \quad \mathbb{E}_{X \sim \rho} \nabla_{\theta} u_{\theta}(X) ((I - P^i)u_{\theta}(X) - (P^b r(X) + T f(X))).$$

An unbiased estimator for (16) is thus

$$(17) \quad \nabla_{\theta} u_{\theta}(X) \left(u_{\theta}(X) - u_{\theta}(X_{\delta}) \mathbf{1}_{\{\delta < \tau\}} - r(X_{\tau}) \mathbf{1}_{\{\delta \geq \tau\}} - \int_0^{\tau \wedge \delta} \frac{f}{a}(X_s) ds \right),$$

where X_s is the solution of (4) at time s with the initial condition given by $X_0 = X$. X_{δ} and X_{τ} are obtained by evaluating X_s at δ and the stopping time τ , respectively. The derivative of the penalty term is

$$(18) \quad 2c \int_{\partial\Omega} \nabla_{\theta} u_{\theta}(x) (u_{\theta}(x) - r(x)) d\mu(x)$$

and an unbiased estimator for the derivative is

$$(19) \quad 2c \nabla_{\theta} u_{\theta}(X) (u_{\theta}(X) - r(X)),$$

where $X \sim \mu$.

The optimization problem (13) and the penalized problem (14) can be solved by applying SGD-type optimization, for example the Adam method in [12]. In the numerical implementation, the integral $\int_0^{\tau \wedge \delta} \frac{f}{a}(X_s) ds$ can be approximated for example by the Euler-Maruyama scheme (see for example [13]). For other implementation details such as the determination of $\mathbf{1}_{\{\delta \geq \tau\}}$, we follow the method in [15]. The complete algorithm is summarized in Algorithm 1.

3. PRIMAL-DUAL FORMULATION FOR EIGENVALUE PROBLEMS

In this section we extend the semigroup method described in Section 2 to a primal-dual algorithm for eigenvalue problems. For the eigenvalue problems, a major difference is that the corresponding variational problem has a constraint $\|u\| = 1$. In [8], the authors divide the neural network approximate solution by a normalization factor when calculating the training loss, which is similar with the Batch Normalization technique, except that the normalization factor is computed with an auxiliary batch rather than the original batch. Here we propose a primal-dual method that handles the constraint via a scalar Lagrange multiplier. As a result, the time complexity of

Algorithm 1 Semigroup method for the elliptic PDE(1)

Require: batch size B and \tilde{B} , total number of iterations T_{iter} , time step δ , learning rate η_t .

1: Initialize the neural network u_θ .

2: **for** $t = 1, \dots, T_{\text{iter}}$ **do**

3: Sample a batch of data from the distribution ρ with size B :

$$X_1, X_2, \dots, X_B \sim \rho.$$

4: For each X_k ($1 \leq k \leq B$), sample $X_{k,\delta}$ according to the SDE (4):

$$X_{k,\delta} = X_k - \nabla V(X_k)\delta + \sqrt{2}W_\delta,$$

and when the periodic boundary condition is used, move $X_{k,\delta}$ into Ω by translating an integer multiple of the period.

5: For each X_k , decide the value of $\mathbf{1}_{\{\delta < \tau\}}$ by

$$\mathbf{1}_{\{\delta < \tau\}} = 1 \text{ if } X_{k,\delta} \in \Omega.$$

6: For each X_k such that $\mathbf{1}_{\{\delta < \tau\}} = 0$, let X_τ be the intersection of $\partial\Omega$ and the line segment $X_k X_{k,\delta}$.

7: Compute the gradient in (17).

8: If the Dirichlet boundary condition is used, sample a batch of data $\{\tilde{X}_j\}_{j=1}^{\tilde{B}}$ from the distribution μ , and compute the gradient of the penalty term by (18).

9: Update the neural network parameters via the Adam method with learning rate η_t (other hyper-parameters in the Adam method are set as the default values).

10: **end for**

solving the eigenvalue problem is only marginally higher than that of solving the corresponding PDE.

By variational principle we know that for the first eigenpair (u, λ) , the eigenvalue problem

$$(20) \quad Lu = \lambda u, \quad \|u\|_{L^2} = 1,$$

with the periodic boundary condition (3) is equivalent to the variational form:

$$(21) \quad u = \operatorname{argmin}_{\|u\|_{L^2}=1} \frac{1}{2} \int_{\Omega} u(x) Lu(x) dx.$$

3.1. Resolving the constraint. The main obstacle in implementing the formulation (21) lies in the constraint $\|u\| = 1$. We propose to handle the constraint with a multiplier term, and reconstruct (21) as the minimax formulation:

$$(22) \quad \min_u \max_g \frac{1}{2} \int_{\Omega} u(x) Lu(x) dx + \frac{g}{2} (\|u\|_{L^2}^2 - 1),$$

where g is the Lagrange multiplier. The equivalence between (21) and (22) can be seen by maximizing over g in (22) and thus we have removed the explicit constraint in (21). We adopt the neural network parameterization as in Section 2 and obtain the following optimization problem:

$$(23) \quad \min_{\theta} \max_g \frac{1}{2} \int_{\Omega} u_{\theta}(x) Lu_{\theta}(x) dx + \frac{g}{2} (\|u_{\theta}\|_{L^2}^2 - 1).$$

Let us define

$$(24) \quad E(\theta, g) = \frac{1}{2} \int_{\Omega} u_{\theta}(x) Lu_{\theta}(x) dx + \frac{g}{2} (\|u_{\theta}\|_{L^2}^2 - 1).$$

Taking derivatives with respect to θ and g gives

$$(25) \quad \begin{aligned} \frac{\partial E}{\partial \theta} &= \int_{\Omega} \nabla_{\theta} u_{\theta}(x) (L + g) u_{\theta}(x) dx, \\ \frac{\partial E}{\partial g} &= \frac{1}{2} (\|u_{\theta}\|_{L^2}^2 - 1), \end{aligned}$$

where we have utilized the symmetry of L .

3.2. Scaling the Lagrange multiplier. In the optimization problem (23), it is important that the Lagrange multiplier has an appropriate scale, since otherwise the problem would be ill-conditioned. If we introduce a scaling parameter c for the dual variable g , then the optimization problem becomes

$$(26) \quad \min_{\theta} \max_g \frac{1}{2} \int_{\Omega} u_{\theta}(x) L u_{\theta}(x) dx + \frac{cg}{2} (\|u_{\theta}\|_{L^2}^2 - 1),$$

or equivalently,

$$(27) \quad E = \frac{1}{2} \int_{\Omega} u_{\theta}(x) L u_{\theta}(x) dx + \frac{cg}{2} (\|u_{\theta}\|_{L^2}^2 - 1),$$

and the derivatives are scaled accordingly:

$$(28) \quad \begin{aligned} \frac{\partial E}{\partial \theta} &= \int_{\Omega} \nabla_{\theta} u_{\theta}(x) (L + cg) u_{\theta}(x) dx, \\ \frac{\partial E}{\partial g} &= \frac{c}{2} (\|u_{\theta}\|_{L^2}^2 - 1). \end{aligned}$$

If c is too large, then in the optimization process the first term in E is neglected by the neural network. If c is too small, then the constraint is not well-enforced. Therefore in the implementation, c should be properly chosen such that the two terms in E are balanced.

Based on (28), we arrive at the gradient descent scheme

$$(29) \quad \begin{aligned} \dot{\theta} &= - \int_{\Omega} \nabla_{\theta} u_{\theta}(x) (L + cg) u_{\theta}(x) dx, \\ \dot{g} &= \frac{c}{2} (\|u_{\theta}\|_{L^2}^2 - 1), \end{aligned}$$

In what follows, we focus on the schrödinger operator $L = -\Delta + V$ and consider the problem of finding the first eigenpair (which corresponds to the ground state) with periodic boundary conditions. The minimax formulation (26) becomes

$$(30) \quad \min_u \max_g \frac{1}{2} \int_{\Omega} |\nabla u(x)|^2 dx + \frac{1}{2} \int_{\Omega} V(x) |u(x)|^2 dx + \frac{cg}{2} (\|u\|_{L^2}^2 - 1).$$

Two stochastic schemes for implementating (29) are discussed below.

3.3. Scheme I. By replacing the operator $\frac{\Delta}{2}$ with the semigroup approximation, we can reformulate (30) as

$$(31) \quad \min_u \max_g \frac{1}{\delta} \int_{\Omega} u(x) (u(x) - \mathbb{E}(u(x + W_{\delta}))) dx + \frac{1}{2} \int_{\Omega} V(x) |u(x)|^2 dx + \frac{cg}{2} (\|u\|^2 - 1),$$

where W_{δ} is the standard Brownian motion. Consider a uniform random variable X on Ω , the problem (31) can be written as

$$(32) \quad \min_u \max_g \frac{1}{\delta} \mathbb{E} u(X) (u(X) - u(X + W_{\delta})) + \frac{1}{2} \mathbb{E} V(X) |u(X)|^2 + \frac{cg}{2} (\|u\|^2 - 1).$$

Since X is uniform on Ω , the process $X + W_{\delta}$ is reversible and

$$(33) \quad \langle u, \tilde{P}v \rangle = \langle \tilde{P}u, v \rangle,$$

where $\langle u, v \rangle = \mathbb{E} u(X) v(X)$ and $\tilde{P}u(x) = \mathbb{E} u(x + W_{\delta})$. By this symmetry, a gradient descent scheme similar with (29) can be derived

$$(34) \quad \begin{aligned} \dot{\theta} &= -\mathbb{E} \nabla_{\theta} u_{\theta}(X) \left(\frac{1}{\delta} (u_{\theta}(X) - u_{\theta}(X + W_{\delta})) + cg u_{\theta}(X) \right), \\ \dot{g} &= \frac{c}{2} \mathbb{E} (u_{\theta}(X)^2 - 1). \end{aligned}$$

Unbiased estimators for the expectations in (34) are therefore

$$(35) \quad \nabla_{\theta} u_{\theta}(X) \left(\frac{1}{\delta} (u_{\theta}(X) - u_{\theta}(X + W_{\delta})) + cg u_{\theta}(X) \right),$$

and

$$(36) \quad \frac{c}{2}(u_\theta(X)^2 - 1),$$

where X is uniform in Ω .

3.4. Scheme II. In (32), we have used $\frac{1}{\delta}(u(x) - \mathbb{E}u(x + W_\delta))$ to approximate $-\frac{\Delta}{2}u(x)$. The effectiveness of this approximation relies on the spatial symmetry of W_δ , which is only true in distribution. In other words, after using the unbiased estimators given in (35) with samples of X and W_δ , the symmetry can be impacted. This problem can be addressed by starting by approximating the first term of (30) with

$$(37) \quad \frac{1}{2} \int_{\Omega} |\nabla u(x)|^2 dx = \frac{1}{2\delta} \left(\int_{\Omega} \mathbb{E}|u(x) - u(x + W_\delta)|^2 dx + o(\delta) \right).$$

The formulation above can be obtained, for example, by plugging $u(x + W_\delta) = u(x) + \nabla u(x) \cdot W_\delta + O(\delta)$ into the expectation, which gives

$$(38) \quad \begin{aligned} \mathbb{E}|u(x) - u(x + W_\delta)|^2 &= \mathbb{E}|\nabla u(x) \cdot W_\delta|^2 + o(\delta) = \mathbb{E}(W_\delta^\top \nabla u(x) (\nabla u(x))^\top W_\delta) + o(\delta) \\ &= \mathbb{E}(\text{tr}(W_\delta^\top \nabla u(x) (\nabla u(x))^\top W_\delta)) + o(\delta) = \mathbb{E}(\text{tr}(\nabla u(x) (\nabla u(x))^\top W_\delta W_\delta^\top)) + o(\delta) \\ &= \text{tr}(\nabla u(x) (\nabla u(x))^\top \mathbb{E}(W_\delta W_\delta^\top)) + o(\delta) = \delta \text{tr}(\nabla u(x) (\nabla u(x))^\top) + o(\delta) \\ &= \delta |\nabla u(x)|^2 + o(\delta). \end{aligned}$$

It is important to see that the factor in front of the integral in (37) is $\frac{1}{2\delta}$, instead of $\frac{1}{\delta}$ in (31).

With this approximation and the uniform random variable X on Ω , (30) can be written as

$$(39) \quad \min_u \max_g \mathbb{E} \left(\frac{1}{2\delta} |u(X) - u(X + W_\delta)|^2 + \frac{1}{2} V(X) |u(X)|^2 + \frac{cg}{2} (u(X)^2 - 1) \right).$$

For this problem, the gradient descent scheme is

$$(40) \quad \begin{aligned} \dot{\theta} &= -\mathbb{E} \left[\frac{1}{\delta} (\nabla_\theta u_\theta(X) - \nabla_\theta u_\theta(X + W_\delta)) (u_\theta(X) - u_\theta(X + W_\delta)) \right. \\ &\quad \left. + \nabla_\theta u_\theta(X) (V(X) u_\theta(X) + cgu_\theta(X)) \right], \\ \dot{g} &= \frac{c}{2} \mathbb{E}(u_\theta(X)^2 - 1). \end{aligned}$$

Unbiased estimators for the expectations are therefore

$$(41) \quad \frac{1}{\delta} (\nabla_\theta u_\theta(X) - \nabla_\theta u_\theta(X + W_\delta)) (u_\theta(X) - u_\theta(X + W_\delta)) + \nabla_\theta u_\theta(X) (V(X) u_\theta(X) + cgu_\theta(X))$$

and

$$(42) \quad \frac{c}{2} (u_\theta(X)^2 - 1).$$

It is clear that even after replacing the expectation with the unbiased estimators, the problem is still symmetric.

3.5. Implementation of the multiplier term. Intuitively, the dual variable should be able to give the correct preference for u_θ . Specifically, when $\|u_\theta\| > 1$, g should be positive, and when $\|u_\theta\| < 1$, g should be negative. In the implementation, this is enforced in each step of the (stochastic) gradient update. We also set the estimation of the gradient of g to be $c/2$ if it is larger than $c/2$. This is because $\frac{c}{2} \mathbb{E}(u_\theta(X)^2 - 1)$ is lower bounded by $c/2$ but it has no upper bound. In practice setting a symmetric upper bound usually gives a better performance. We summarize the implementation details in Algorithm 2, where we adopt the neural network architecture in Figure 2.

Algorithm 2 Semigroup methods for the eigenvalue problem.

Require: threshold of the dual variable g_{thresh} , batch size B and \tilde{B} , total number of iterations T_{iter} , time step δ , learning rate $\eta_t, \tilde{\eta}_t$, scaling factor c .

- 1: Initialize the neural network u_θ .
 - 2: **for** $t = 1, \dots, T_{\text{iter}}$ **do**
 - 3: Sample a batch of data $\{X_k\}_{k=1}^B$ uniformly in Ω .
 - 4: Compute the gradient in (35) or (41).
 - 5: Sample a batch of data $\{\tilde{X}_j\}_{j=1}^{\tilde{B}}$ uniformly in Ω .
 - 6: Compute $\epsilon_t = \max\left(\sum_j u_\theta(\tilde{X}_j)^2 - 1, 1\right)$.
 - 7: **if** $t = 1$ **or** $\epsilon_t \epsilon_{t-1} < 0$ **then**
 - 8: Set $g = \text{sign}(\epsilon_t) g_{\text{thresh}}$.
 - 9: **else**
 - 10: Update the dual variable by $g \leftarrow g + \tilde{\eta}_t \frac{c \epsilon_t}{2}$.
 - 11: **end if**
 - 12: Update the neural network parameters by the Adam method with learning rate η_t (other hyper-parameters in the Adam method are set as the default values).
 - 13: **end for**
-

4. NUMERICAL EXPERIMENTS

4.1. Elliptic PDEs. In the first numerical example, we set $a = 1$ in (1) and hence the PDE is the Lapacian equation. This example is a good starting point for verifying the effectiveness of the treatment of a non-zero right-hand-side term, which is a case not covered in [15]. We let the right-hand-side term $f = -2d$ and assume the Dirichlet boundary condition (2) with $r(x) = 1$ on the boundary of the domain $\Omega = B(0, 1)$, the unit ball in \mathbb{R}^d . The ground truth is then simply $u(x) = \|x\|^2$. When $d = 10$, 1.0×10^6 samples are used to train the neural network. After a training process of 6000 epochs, the final error $\|u_\theta - u^*\|_{L^2_\rho(\Omega)} / \|u^*\|_{L^2_\rho(\Omega)}$ is 0.036, which is a clear indication that the numerical scheme (13) is able to solve the problem with non-zero right-hand-side term.

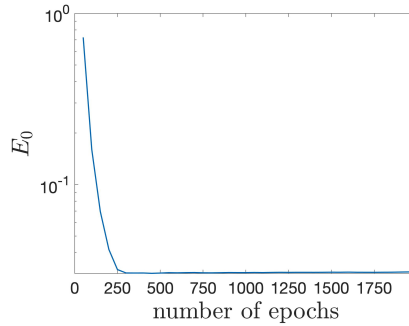


FIGURE 3. The error of the numerical solution in the process of training.

In the second numerical example, we consider a problem with the periodic boundary condition. The parameters are

$$(43) \quad \begin{aligned} a(x) &= \exp\left(-\sum_{i=1}^d \cos(2\pi x_i)\right), \\ f(x) &= 2\pi^2 \exp\left(-\sum_{i=1}^d \cos(2\pi x_i)\right) \left(\sum_{i=1}^d (2 \sin(2\pi x_i) - \sin(4\pi x_i))\right). \end{aligned}$$

By direct calculation, we see that the exact solution is

$$(44) \quad u(x) = \sum_{i=1}^d \sin(2\pi x_i)$$

When $d = 10$, 1.0×10^7 samples are used to train the neural network. After a training process of 2000 epochs, the final error $\|u_\theta - u^*\|_{L^2_\rho(\Omega)} / \|u^*\|_{L^2_\rho(\Omega)}$ is 0.031. The evolution of the precision of the approximate solution is demonstrated in Figure 3, which shows a rapid convergence of the numerical solution.

4.2. Eigenvalue problem - Schrödinger operator. In this section, we consider the eigenvalue problem associated with the Schrödinger operator

$$(45) \quad L = -\Delta + V,$$

and the periodic boundary condition (3). Here V is a potential function

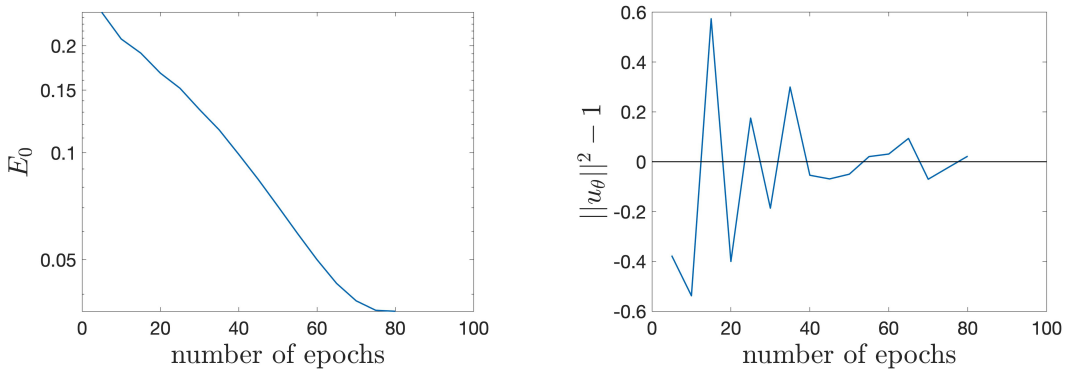
$$(46) \quad V(x) = 4\pi^2 \sum_{i=1}^d c_i \cos(2\pi x_i),$$

where $c_i \in [0, 0.2]$ for $1 \leq i \leq d$. We adopt the same parameters as in [8]. The reference solution u^* is obtained by the spectral method described in [8]. Numerical tests are performed when $d = 5, 10$.

4.2.1. Scheme I. When adopting the semigroup formulation (31), 1.6×10^6 samples are used to train the neural network with width 600 and 80 epochs of training is implemented. Throughout the training process, the learning rate $\tilde{\eta}_t = \eta_t = 0.0008$. The hyper-parameters g_{thresh} and δ are set to be 1 and 0.001, respectively. For the 5-dimensional case, the scaling factor is $c = 50$ and for the 10-dimensional case it is $c = 40$.

The training process for the 5-dimensional case and the 10-dimensional case are presented in Figure 4 and Figure 5. The final errors are 0.036 and 0.051, respectively. From Figure 4(a) and Figure 5(a) it can be seen that the numerical solution converge to the reference solution, and the constraint $\|u_\theta\| = 1$ is well-enforced at the end of the training process, as shown in Figure 4(b) and Figure 5(b).

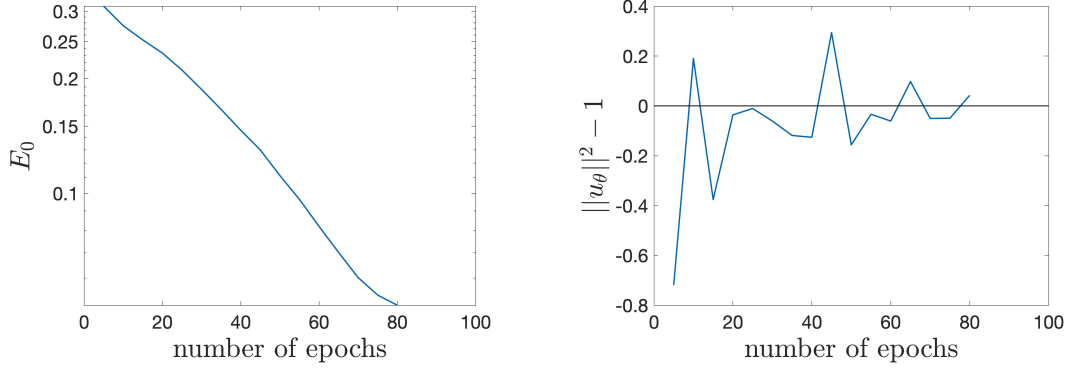
Since it is difficult to visualize functions in high dimensions, we compare the probability density function of $u_\theta(Z)$ and $u(Z)$, where Z is a uniform random variable on Ω . The probability density function is obtained by performing kernel density estimation on a sample set of size 10000. The comparison of the probability density functions are given in Figure 6, from which we can conclude that the numerical solutions obtained are in good accordance with the ground truths.



(a) The error of the numerical solution in the process of training.

(b) The residue $\|u_\theta\|^2 - 1$ of the constraint in the process of training.

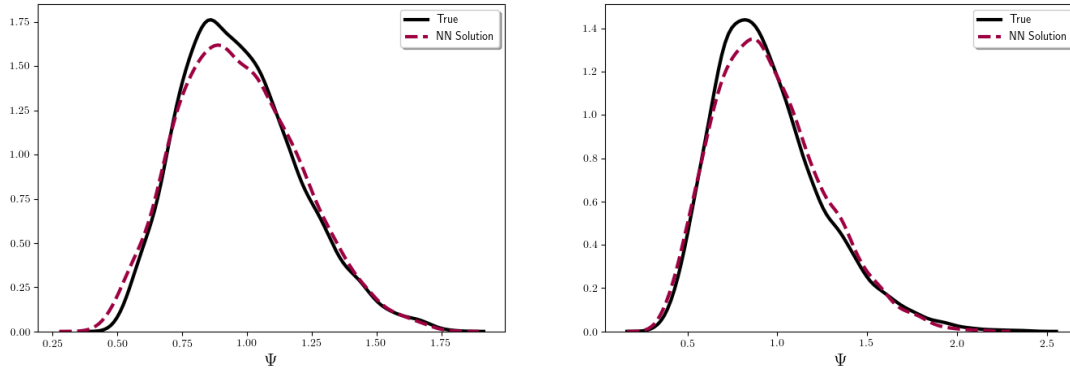
FIGURE 4. The convergence of the error E_0 and the residue of the constraint $\|u_\theta\|^2 - 1$ in the training process of the 5-dimensional problem.



(a) The error of the numerical solution in the process of training.

(b) The residue $\|u_\theta\|^2 - 1$ of the constraint in the process of training.

FIGURE 5. The convergence of the error E_0 and the residue of the constraint $\|u_\theta\|^2 - 1$ in the training process of the 10-dimensional problem.



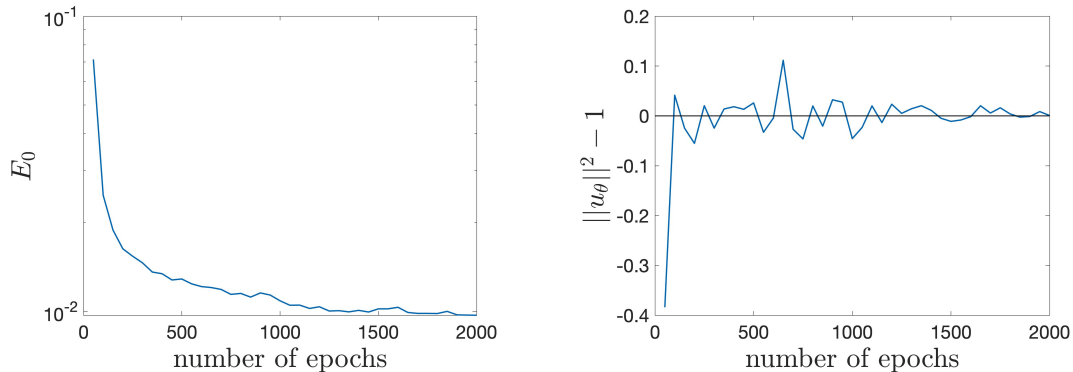
(a) Comparison of the 5d result.

(b) Comparison of the 10d result.

FIGURE 6. Comparisons between the NN represented solutions and the ground truths using semigroup scheme I. (a): The 5-dimensional case. (b): The 10-dimensional case.

4.2.2. *Scheme II.* When adopting the semigroup formulation (39), 4.0×10^6 samples are used to train the neural network with width 600, and 2000 epochs of training is implemented. In this case, the hyper-parameter δ and g_{thresh} are set to be 0.001 and 4 respectively, and the scaling factor c is 10. The learning rate for the dual variable $\tilde{\eta}_t$ is set as 0.1 while the learning rate for the primal variable η_t is set as 0.0008 for the first half of the training process and 0.0003 for the second half of the training process.

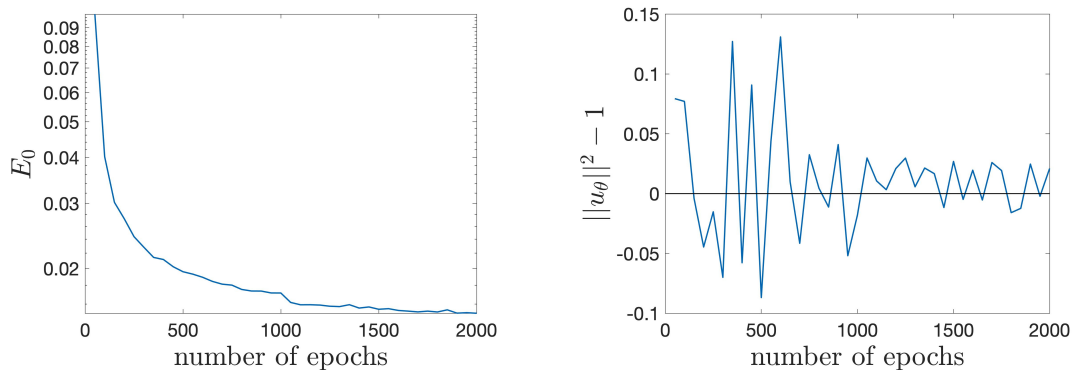
For the 5-dimensional case and the 10-dimensional case, the final errors are 0.0097 and 0.015, respectively. The training process are depicted in Figure 7 and Figure 8, respectively. As illustrated in Figure 7(a) and Figure 8(a), the numerical solutions converge to the corresponding reference solutions. Compared with the training process using Scheme I, the final errors are much lower, although it takes more epochs to reach the final precision. This can also be verified by comparing Figure 6 and Figure 9, since the estimated probability density functions for the numerical solutions are closer to the probability density functions for the reference solutions in Figure 9. We check that the constraint $\|u_\theta\| = 1$ is well-enforced at the end of the training process in Figure 7(b) and Figure 8(b).



(a) The error of the numerical solution in the process of training.

(b) The residue $\|u_\theta\|^2 - 1$ of the constraint in the process of training.

FIGURE 7. The convergence of the error E_0 and the residue of the constraint $\|u_\theta\|^2 - 1$ in the training process of the 5-dimensional problem.



(a) The error of the numerical solution in the process of training.

(b) The residue $\|u_\theta\|^2 - 1$ of the constraint in the process of training.

FIGURE 8. The convergence of the error E_0 and the residue of the constraint $\|u_\theta\|^2 - 1$ in the training process of the 10-dimensional problem.

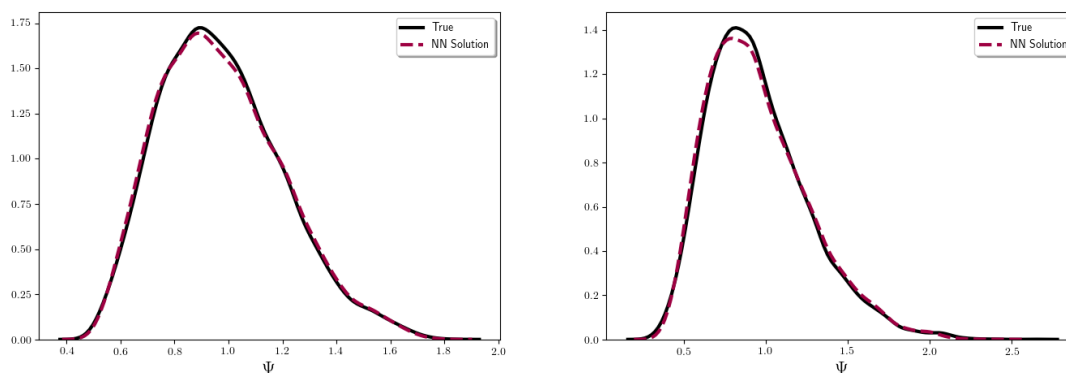
5. CONCLUSION

In this paper, we present a semigroup method solving high dimensional PDE problems and eigenvalue problems effectively. We have shown numerically the efficiency of the proposed method in problems that have non-zero right-hand-side term with Dirichlet boundary conditions and periodic boundary conditions. Two semigroup schemes are proposed for the eigenvalue problems. With a scalar Lagrange multiplier, these schemes are able to handle the constraint in the eigenvalue problem and obtain accurate solutions.

The numerical schemes adopted here are generally first-order schemes. For future work, higher order schemes can be applied to improve the precision. Moreover, importance sampling techniques can be integrated with the proposed method to facilitate the generation of a training set with high quality.

REFERENCES

- [1] Mohammed AlQuraishi, *AlphaFold at casp13*, *Bioinformatics* **35** (2019), no. 22, 4862–4865.



(a) Comparison of the 5d result.

(b) Comparison of the 10d result.

FIGURE 9. Comparisons between the NN represented solutions and the ground truths using Scheme II. (a): The 5-dimensional case. (b): The 10-dimensional case.

- [2] Giuseppe Carleo and Matthias Troyer, *Solving the quantum many-body problem with artificial neural networks*, *Science* **355** (2017), no. 6325, 602–606.
- [3] Jacob Devlin, Ming-Wei Chang, Kenton Lee, and Kristina Toutanova, *Bert: Pre-training of deep bidirectional transformers for language understanding*, arXiv preprint arXiv:1810.04805 (2018).
- [4] Weinan E, Jiequn Han, and Arnulf Jentzen, *Deep learning-based numerical methods for high-dimensional parabolic partial differential equations and backward stochastic differential equations*, *Communications in Mathematics and Statistics* **5** (2017), no. 4, 349–380.
- [5] Weinan E and Bing Yu, *The deep ritz method: a deep learning-based numerical algorithm for solving variational problems*, *Communications in Mathematics and Statistics* **6** (2018), no. 1, 1–12.
- [6] WMC Foulkes, Lubos Mitas, RJ Needs, and Guna Rajagopal, *Quantum monte carlo simulations of solids*, *Reviews of Modern Physics* **73** (2001), no. 1, 33.
- [7] Alex Graves, Abdel-rahman Mohamed, and Geoffrey Hinton, *Speech recognition with deep recurrent neural networks*, 2013 IEEE International Conference on Acoustics, Speech and Signal Processing, 2013, pp. 6645–6649.
- [8] Jiequn Han, Jianfeng Lu, and Mo Zhou, *Solving high-dimensional eigenvalue problems using deep neural networks: A diffusion monte carlo like approach*, *Journal of Computational Physics* **423** (2020), 109792.
- [9] Kaiming He, Xiangyu Zhang, Shaoqing Ren, and Jian Sun, *Deep residual learning for image recognition*, Proceedings of the IEEE conference on computer vision and pattern recognition, 2016, pp. 770–778.
- [10] Weile Jia, Han Wang, Mohan Chen, Denghui Lu, Jiduan Liu, Lin Lin, Roberto Car, Linfeng Zhang, et al., *Pushing the limit of molecular dynamics with ab initio accuracy to 100 million atoms with machine learning*, arXiv preprint arXiv:2005.00223 (2020).
- [11] Yuehaw Khoo, Jianfeng Lu, and Lexing Ying, *Solving for high-dimensional committor functions using artificial neural networks*, *Research in the Mathematical Sciences* **6** (2019), no. 1, 1.
- [12] Diederik P Kingma and Jimmy Ba, *Adam: A method for stochastic optimization*, arXiv preprint arXiv:1412.6980 (2014).
- [13] Peter E Kloeden and Eckhard Platen, *Numerical solution of stochastic differential equations*, Vol. 23, Springer Science & Business Media, 2013.
- [14] Alex Krizhevsky, Ilya Sutskever, and Geoffrey E. Hinton, *Imagenet classification with deep convolutional neural networks*, *Commun. ACM* **60** (May 2017), no. 6, 84–90.
- [15] Haoya Li, Yuehaw Khoo, Yinyu Ren, and Lexing Ying, *Solving for high dimensional committor functions using neural network with online approximation to derivatives*, arXiv preprint arXiv:2012.06727 (2020).
- [16] Maziar Raissi, Paris Perdikaris, and George E Karniadakis, *Physics-informed neural networks: A deep learning framework for solving forward and inverse problems involving nonlinear partial differential equations*, *Journal of Computational Physics* **378** (2019), 686–707.
- [17] Linfeng Zhang, Jiequn Han, Han Wang, Roberto Car, and Weinan E, *Deep potential molecular dynamics: a scalable model with the accuracy of quantum mechanics*, *Physical review letters* **120** (2018), no. 14, 143001.